Volume 19, Number 2, 2026. pp. 249-264

Jordan Journal of Physics

ARTICLE

Dynamics and Conformational Shifts of d(GGGGTTTTGGGG)$_4$ DNA Quadruplex: A Molecular Dynamics Simulation Study

Jwala Ji Prajapati[a], **Ramesh Kumar Yadav**[b] and **Umesh Yadava**[a]

[a] *Department of Physics, Deen Dayal Upadhyaya Gorakhpur University, Gorakhpur, 273009, U.P., India.*

[b] *Department of Physics, B.R.D. Post Graduate College, Deoria, 274001, U.P., India.*

DOI: **https://doi.org/10.47011/19.2.11**

Received on: 11/02/2025; *Accepted on: 29/05/2025*

Abstract: This study investigated the molecular dynamics (MD) simulation and conformational analysis of a DNA quadruplex, whose crystal structure has been previously reported. The initial coordinates for the DNA quadruplex were sourced from the Protein Data Bank (PDB ID: 1d59), containing the sequence d(GGGGTTTTGGGG)$_4$ from *Oxytricha trifallax*. This telomeric sequence forms a complex composed of two d($G_4T_4G_4$) strands, stabilized by cyclic hydrogen bonding between four guanine bases to form G-quartets. Following the generation of the DNA quadruplex model, a molecular dynamics simulation was conducted using OPLS4 force field over a duration of 100 ns at 300 K. Trajectories of the dynamic pathway were examined at intervals of 10 ns. Structural and conformational changes over a time span of 100 ns were analyzed using the X3DNA software, focusing on RMSD and RMSF plots. The resulting data was compared with the known crystal structure of the DNA quadruplex. The molecular dynamics simulation showed that at 300 K the quadruplex retained its B-type DNA conformation (as the original structure parameters) but with slight structural variations suggesting potential therapeutic relevance. Additionally, Principal Component Analysis (PCA) applied to the simulation trajectory yielded important insights regarding the DNA quadruplex, indicating its properties under different physiological conditions. These findings could be helpful for further studies on the interaction of DNA quadruplexes with external agents and ligands, contributing to a better understanding of their interaction capabilities.

Keywords: G-quadruplex telomere, MD simulation, Torsional and Helicoidal parameters, Non-canonical DNA, *Oxytricha trifallax*, X3DNA.

1. Introduction

In molecular biology, alternative DNA G-quadruplex secondary structures (G4s) are formed by guanine-rich sequences [1]. These structures are primarily formed at telomeric regions of chromosomes as higher-order DNA non-canonical secondary structure folded into one-, two-, or four-stranded helical structures [2]. Telomeres are located at the ends of chromosomes and contain stabilized DNA quadruplex sequences, where they play a very important role in maintaining chromosomal stability and integrity of living cell chromosomes which show unique properties. In ciliated protozoan *Oxytricha trifallax*, the macronuclear telomere ends exhibit distinct structural properties that facilitate sequence progression. In the telomere region of the Oxytricha, the sequence reported by Lipps et al. (1982) is: 5'-$C_4A_4C_4A_4C_4$-----$G_4T_4G_4T_4G_4T_4G_4T_4G_4$-3' [3]. Oxytricha possesses the sequence d(GGGGTTTTGGGG)$_4$ which forms hairpin-like structures for the building of a four-stranded structure which is helical in shape having loops involving four thymine residues at either end [4]. The telomeric sequence involving two d($G_4T_4G_4$) molecules associated with cyclic hydrogen

Corresponding Author: Umesh Yadava **Email**: umesh.phy@ddugu.ac.in

bonding among four guanines. Loops form at opposite ends of the molecule due to two thymine tracts, which connect G tracts on the same side rather than diagonally. This arrangement creates two extensive and two contracted grooves; the narrow grooves are formed by either two 5' ends or two 3' ends. This structure may facilitate the binding of two identical polynucleotide chains, as seen in the genomic copies present in all retroviruses, including HIV [3, 4].

G4 DNA structures can exist in unimolecular or multimolecular forms and adopt different topologies depending on strand interactions. These interactions form a parallel square-planar structure known as a G-tetrad. G4 association does not rely solely on base pairing but is also influenced by hydrogen-bonding patterns [3]. Each G-tetrad contains four guanines, and the hydrogen bonds act as bridges between donor and acceptor atoms. Thus, all four guanines are held together via a Hoogsteen type H- bonding. Four guanines in each segment have glycosyl conformations that can vary between syn and anti. "*Syn*" and "*anti*" conformations describe the relative orientations of substituents around a double bond or within a ring system. In the '*syn'* conformation, the substituents are positioned on the same side, whereas in the '*anti'* conformation they lie on opposite sides. The tetrads (G-Quartet) stack on each other and further becomes stable by introducing centrally coordinated physiological monovalent metal cations like K^+, Na^+, Li^+, etc in the cavity, which can stabilize G-quadruplex structures. Ions are critical in supporting and stabilizing G-quadruplex structures, playing a distinct role in telomere maintenance, DNA replication, and the regulation of gene expression at both the transcriptional and translational levels. These structures contribute to genome stability and are involved in the expression of oncogenes in eukaryotic genomes, as well as in various organisms, including some bacterial pathogens [5], non-pathogenic bacteria, viruses [6] and certain plant species [7-9].

G4 structure formation can contribute to genome instability by inducing mutations, deletions, and promoting recombination events. To date, nearly 2800 different molecules (G4 ligands) are produced which have been used to target G4 structures. Many G4 ligands exhibit an aromatic surface that stack with the outer G-tetrads, along with a positive charge or basic groups that interact with the grooves or loops of G-quadruplex structures. These ligands also have structural features that prevent intercalation with double-stranded DNA. Although they may lack traditional drug-like characteristics, G4-interactive binding ligands can influence G-quadruplex structures, thereby disrupting vital DNA processes such as replication and transcription. This disruption can lead to single-strand (SSBs) and double-strand breaks (DSBs), activating the DNA damage response (DDR) machinery [10].

G4s play significant regulatory functions in essential viral processes in viruses. Recent research has demonstrated the involvement of G4 structures in pathogens associated with serious diseases, including Mycobacterium tuberculosis (Mtb), cancer, Pseudomonas aeruginosa, human papillomavirus (HPV), human immunodeficiency virus (HIV) and SARS-CoV-2 [11-13]. G-quadruplex structures exhibit distinct characteristics both in vitro and in vivo when analyzed using various biophysical techniques [14, 15]. Many experiments on G4 quadruplex of different species have demonstrated that G4 structures can inhibit abnormal development of cells and tissues and telomere elongation of cancer cells, tumour cells, neurological disorders, mycobacterium tuberculosis (*Mtb*), and other pathogenic disease [16, 17]. Once the pattern of G-quadruplex gets broken one can prevent the mutation of genes and allow ligands or drugs to interact with it to modulate its biological activity through pharmacological interactions [18-20].

The structural diversity allowed us to modulate the comparative studies between crystal structures which may be used in detecting the problems that can influence the biological activities. The sequence was modelled and went through the MD simulations for predictive studies. Currently, various computational and experimental atomistic techniques are available to confirm the G4-appearance capability of sequences. Some methods offer insights into the thermal stability of quadruplexes to satisfy the limitations and structural parameters [21-24] but none of these techniques are suitable for understanding and recognizing the new type of G-quadruplex. MD simulations provide detailed atomic-level information on molecular dynamics occurring over microsecond and millisecond

timescales that are difficult to capture experimentally [25-28]. The $d(GGGGTTTTGGGG)_4$ DNA sequence adopts a G-quadruplex structure that exhibits significant dynamic behavior, characterized by conformational flexibility and transitions between different stacking arrangements and loop configurations over time [29]. *Oxytricha trifallax* is chosen for molecular dynamics (MD) simulations of the $G_4T_4G_4$ DNA quadruplex because it possesses a well-characterized telomeric sequence, $d(G_4T_4G_4)$, that readily forms stable *G-quadruplex structures*. These sequences are naturally found at the ends of *Oxytricha* chromosomes and have been extensively studied experimentally, however, the computational studies are rare. The present study aims to investigate the structural dynamics and biophysical conformation of the telomeric G-quadruplex DNA sequence $d(G_4T_4G_4)_4$ from *Oxytricha trifallax* using MD simulations, with the goal of gaining insight into its conformational flexibility, stability, and potential as a target for ligand interaction.

2. Methodology

2.1. Explicit Molecular Dynamics Simulation

The three-dimensional structure of the G-quadruplex of the sequence $d(GGGGTTTTGGGG)_4$ was obtained from the PDB entry 1D59 [4]. Initially, the DNA G-quadruplex was protonated at pH (7 ± 0.5), using Protein Preparation Wizard of the Schrodinger Suite and placed in Monte-Carlo equilibrated explicit transferable intermolecular potential (TIP4P) solvent, a rigid four-site model featuring three fixed point charges and a single Lennard-Jones center [30]. A $10\times10\times10$ $Å^3$ buffer simulation grid box was used.

The system was fully charge-neutralized by adding an appropriate number of counterions using the system-building feature of the DesmondV4.4 package [31] under a Linux environment on an HP Z2 workstation configured with a 4-core Intel Xeon E-2244G processor, 4.8 GHz base frequency with Intel Turbo Boost Technology, 16 GB RAM and 1 NVIDIA Quadro P2000-5 GB GDDR5 graphic card. The simulation box contained 1564 atoms, excluding water molecules. The entire system underwent energy minimization using the steepest descent method until reaching a slope threshold of 24.8 kcal/mol-Å. This was followed by conjugate-gradient energy minimization under physiological conditions through molecular dynamics simulations, achieving an acceptable Root Mean Square (RMS) gradient of 0.1 kcal/mol-Å. Random velocities corresponding to a Boltzmann distribution at 100 K were assigned to all atoms and the system temperature was gradually increased from 100 K to 300 K over 2.0 ps by scaling under constant pressure. The equilibration protocol involved a two-stage process: initially, the system was subjected to an NVT ensemble (constant number of particles, volume, and temperature) to stabilize the temperature, followed by an NPT ensemble (constant number of particles, pressure, and temperature) to stabilize the pressure and density. Temperature was maintained at 300 K using the Nosé–Hoover thermostat, while pressure was controlled at 1 atm using the Martyna–Tobias–Klein barostat [31]. After equilibration, the system was subjected to a 100 ns MD production run under an NPT ensemble using the OPLS4 all-atom force field as implemented within the Desmond software [32, 33]. OPLS4 is a highly optimized force field that provides a balanced combination of accuracy and efficiency, making it suitable for a broad range of simulations, especially those involving biomolecules, solvents, and complex molecular systems [34]. Desmond uses periodic boundary conditions (PBCs) by default to replicate an infinite system, ensuring that edge effects do not distort the simulation. Long-range Coulombic interactions were evaluated using the Particle Mesh Ewald (PME) approach. The PME method is a computational technique that improves upon the regular Ewald approach by mapping charges onto a grid (mesh) and using fast Fourier transforms (FFT) to efficiently calculate the long-range interactions, making it well-suited for systems with many charged particles, such as proteins, DNA, and other biomolecules [35]. The Verlet leapfrog algorithm was employed during the simulation with a 1.0 fs time step duration for minimization and 2.0 fs for dynamics. The Verlet leapfrog algorithm is a widely used numerical method in MD simulations for updating particle positions and velocities over time. It solves the equations of motion by updating positions and velocities in an interleaved manner, enhancing stability and accuracy in time-dependent simulations [36]. During the MD simulation, the Berendsen

algorithm was applied to maintain constant temperature and pressure. Snapshots were taken at periodic intervals of 10 ns during the MD Simulation. Following the simulations, the trajectories were examined through statistical mechanics approaches, including root mean square deviation (RMSD) and root mean square fluctuation (RMSF) for each DNA G-quadruplex chain. RMSD measures the average displacement of a selected group of atoms in each frame relative to a reference frame and is calculated across all frames of the trajectory. RMSF describes how much each residue fluctuates around its average position over time. Whereas RMSD measures overall structural deviation over time (comparing whole structures), RMSF focuses on the extent to which each individual residue fluctuates around its mean position. Principal component analysis (PCA) was also carried out by means of the Bio3D package in the R environment (https://www.r-project.org/) [37, 38]. PCA is a statistical method used in molecular dynamics to identify major patterns of motion in molecules like proteins or DNA. It involves constructing a covariance matrix of atomic positional fluctuations, then diagonalizing it to obtain eigenvectors (motion directions) and eigenvalues (extent of motion along each direction). The first principal component (PC1) captures the largest collective motion, while PC2, PC3, and subsequent components describe smaller but important movements. Typically, the first few principal components account for most biologically relevant motions [39].

2.2 Conformational Analysis of DNA G-quadruplex

DNA quadruplexes are dynamic molecules capable of adopting multiple non-canonical conformations to adopt alternative conformations essential for various biological functions. In our analysis, we utilized X3DNA to calculate backbone and helicoidal parameters [40, 41]. For this study, we extracted 10 snapshots at 10 ns intervals across a 100 ns molecular dynamics simulation. These parameters were assessed to characterize structural flexibility in the DNA, focusing on parameters such as axis bend angles, slide, roll, twist, rise, and groove widths.

X3DNA is capable of handling various nucleic acid structures, including antiparallel and parallel double helices, single-stranded structures, triplexes, quadruplexes, and other complex tertiary motifs in both DNA and RNA. Its analysis routines identify and classify fundamental interactions while characterizing the double-helical nature of relevant base pair steps. The program employs reference frames to describe nucleic acid base-pair geometry and utilizes a rigorous matrix-based approach to compute local conformational parameters, enabling structure reconstruction. Helicoidal and torsion angle parameters play a critical role in understanding base folding and rotation during dynamic processes [40, 41].

3. Results and Discussion

3.1 The Dynamic Behavior of DNA G-quadruplex Structure

The crystallographic structure of the *oxytricha trifallax* DNA G-quadruplex model consists of guanine-rich quartets associated to form a square-planar secondary structure with non-Watson-Crick base pairing. The planes of the tetrad stack on top of each other in a parallel form which determines the folding of G4 structures and formed a stabilized model in the presence of central physiological cations. The analysis of the quadruplex demonstrated that it can adopt a range of topologies based on nucleotide arrangements. Investigations of the G-quadruplex can be done by computational simulation programs [42-44]. The synergistic interplay of Hoogsteen hydrogen bonds, π–π stacking with van der Waals contributions, and specific cation coordination is essential for the formation and stability of G-quadruplex structures. Disruption of any one of these interactions through thermal fluctuations, absence of stabilizing ions, or sequence mutations can lead to destabilization or unfolding of the G4 motif [45, 46]. To investigate the thermodynamic stability of the selected DNA quadruplex in solution, fully atomistic MD simulations were initially performed. The conformational properties of the simulated models were then compared with the corresponding experimental crystal structure [47-49]. Snapshots taken at 10 ns intervals during the 100 ns simulation at 300 K demonstrated steady behavior, particularly in the planar region of the quadruplex (Fig. 1). Examination of these snapshots highlighted flexibility in the base pairs, mainly located on the edges of the square planar quartet. At this

temperature, no significant disturbances were observed, indicating that the system remained stable without any abrupt fluctuations. Minor folding of the strands was also noted, with the guanine base planes slightly adjusting in relation to neighboring bases, leading to closer interactions. These slight conformational adjustments enhance the robustness of the G-quadruplex structure without compromising its core stability. They enable adaptability, promote interaction with ligands, and maintain structural integrity under physiological fluctuations — all essential for their biological roles and for designing drugs targeting them.

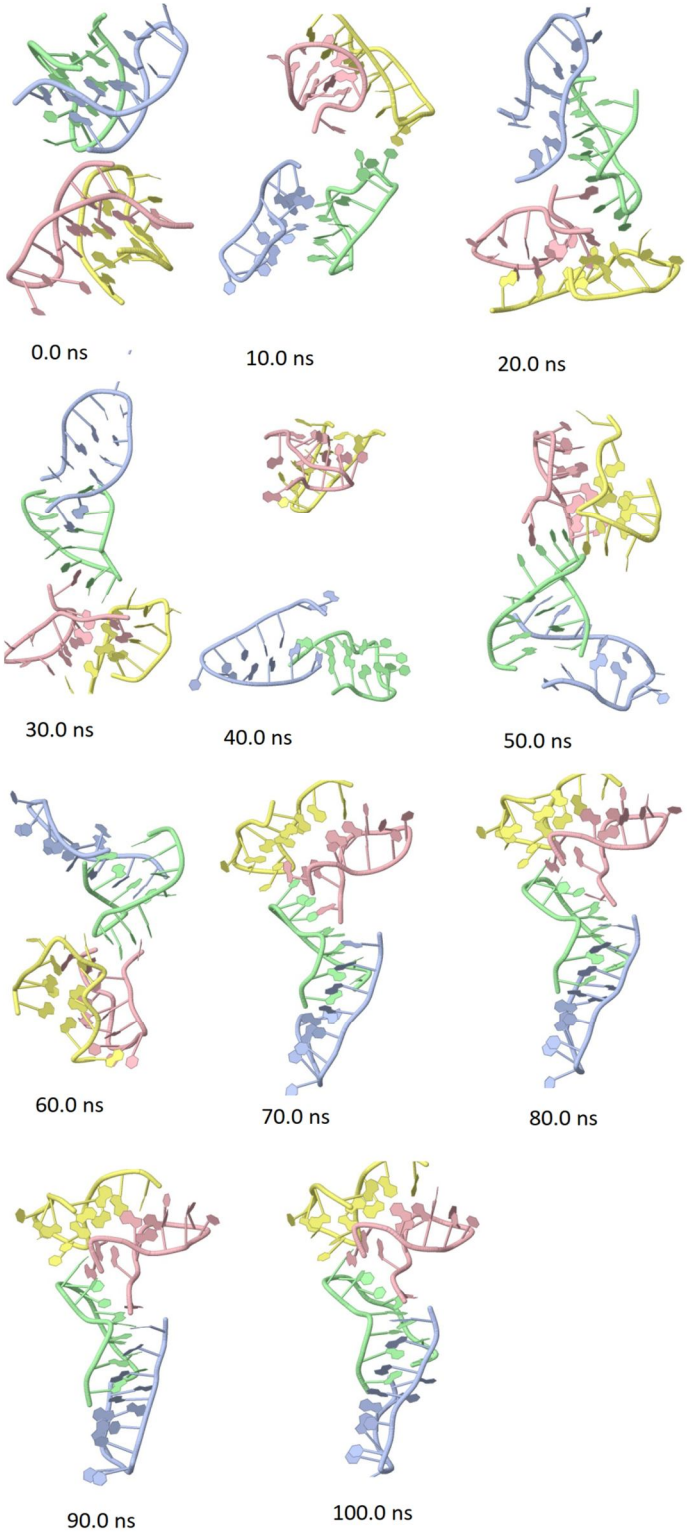

FIG. 1. Snap shots at every 10.0 ns of molecular dynamics production run.

3.2 Torsion Angle Parameters Analysis

Moreover, the backbone torsion angles (α, β, γ, δ, ε, ζ, η, and χ) for each nucleotide in the DNA quadruplex model were calculated. These angles define the relative orientation of atoms around bonds, impacting overall structure and shape of the DNA molecule. These torsion angles describe the backbone of the DNA molecule connecting the sugar and phosphate groups. α, β and γ angles have trimodal distributions with gauche (-) ($300^o \pm 30^o$), gauche (+) ($60^o \pm 30^o$) and trans ($180^o \pm 30^o$) conformations being common. The calculated values of torsion angles are depicted in given tables. Supplementary Tables S1 & S2 shows the initial structure, i.e., pre-dynamics [50] while Table 1 & 2 shows the torsion angles obtained from the MD simulation at 300 K over 100 ns are presented. The terms ±Gauche (±g) and trans (t) describe the broad conformational range, while more detailed analysis is done using Klyne-Prelog notation, including syn, anti, synclinal (sc), and anticlinal (±ac) *etc*. The data shows a notable linked conformational behaviour between torsion angles α, where the first and second strands primarily oscillate between the gauche (g-) and gauche (g+) regions for most residues.

Symmetric nonappearance of torsion angles α for residues 3G of the first strand and residues 8G of the second strand are obtained. Similar symmetric deficiencies of torsion angles β are found for the residues 3G and 5G, respectively. Missing values for backbone and glycosidic torsion angles generally occur due to disorder in the structure at that particular site. The torsion angle γ shows considerable dynamic transitions within the *trans* regions for the majority of the first and second strand residues, δ shows anticlinal (ac) regions for first and second strands both. The torsion angles ε and ζ fluctuate freely between the gauche (g−) and -synclinal (-sc) regions for both strands. Similar patterns are observed for the glycosidic angle (χ), it fluctuates throughout the trajectory between the –ac and –ap regions for most of the residues for first and second strands of the molecule with the exception of G5, G10 and G15 which are in g^+, t^+, g^+ respectively [50]. Significant dynamic fluctuations are observed in the sugar rings into the C2′-exo to C2′-endo regions for the first and second strands respectively. It indicates that structural integrity is maintained throughout the dynamics. After dynamics, most of the sugar rings are oscillating in C1′ exo to C1′ exo regions. By comparing the conformational parameters derived from the X3DNA program for the original structure with the standard values for various DNA types, it is observed that while there are variations between the original and MD simulated structures, the parameters fall within the expected ranges for B-type DNA.

Analysis of torsion angles post-MD simulation showed that χ angles remained within syn and anti-regions, preserving G-quadruplex topology. Minor γ and δ fluctuations indicated local flexibility, while stable ε and ζ angles reflected a rigid phosphate backbone, supporting overall structural stability. This indicates that the torsion angles configurations contribute to the stability of different DNA conformations and they play a crucial role in various DNA functions, including replication, transcription, and ligand binding.

TABLE 1. Torsion angle parameters of strand-I for the final structure of 100 ns dynamics

S.N.	base	*alpha*	*beta*	*gamma*	*delta*	*epsilon*	*zeta*	*chi*
1	G	-74.4	44.4	176.2	118.5	-81.7	-55	-119
2	T	-84.4	65.8	175.6	99	-86.1	-128.8	-121.2
3	G	--	--	-150	151.6	-85.6	75.2	-176.2
4	G	82.6	-95.1	-167.6	129.8	-85.2	-82.3	-122.1
5	G	-27.7	-62.4	-145.6	110.6	-107.4	-74.1	62.4
6	G	-79.6	52.5	164.4	143.8	-94.7	-69.7	-112.5
7	T	-42.6	-45.4	-157	99.7	-103.3	-61.5	-118.8
8	G	-81.1	54.7	178	111.2	-69.3	-56.1	-67.2
9	G	56.8	177.3	179.2	154.8	-94.2	-73.5	167.8
10	G	-77.6	50.6	160.9	138	-55.4	-130.3	-130.1
11	G	71.6	76.7	178	120	-94.2	-93.3	-144.4
12	G	77	-84.6	-175.3	100.2	48.1	-86.3	-110.3
13	G	-73.7	51.1	171.1	116.1	-84.9	-76.6	-127.9
14	G	-94.2	73.5	130.9	108	-62.4	-53.6	56.5

TABLE 2. Torsion angle parameters of strand-II for the final structure after 100 ns dynamics

S.N.	base	*alpha*	*beta*	*gamma*	*delta*	*epsilon*	*zeta*	*chi*
1	G	-86.8	58.2	168.1	134.3	-92.1	-61.2	59.3
2	T	75.6	98.5	179.9	104.7	-86.5	-84.8	-48.7
3	G	83.4	-80.5	-158.8	97.4	--	….	-122.5
4	G	-93	54	170.9	127.6	-75.4	-137.9	62.4
5	G	78.5	-112.9	-162.2	87.3	-110.7	-57.6	-150.5
6	G	112.9	76.3	-176.9	154.6	-73.5	88.9	-173.1
7	G	-62.6	26.8	-162.6	70.8	--	--	-105.8
8	G	--	….	173.5	135.4	-99.3	-55.6	-140.5
9	G	-80.5	55.9	151	120.4	-80.9	-52.3	-139
10	G	-80.6	36.1	-178.4	142.3	-97.1	-90.4	-82.8
11	T	-79.3	57	157.9	102.1	-85.2	-54.4	-145.2
12	T	-67.2	6.7	-176.1	86	-155.7	-60.7	54.1
13	T	-75.2	75.6	175.4	121.1	-82.7	-164.2	168.2
14	G	-69.9	30.9	-176.2	128.4	-85.2	-109.7	-116.7

3.3. Helix Axis Parameters Analysis

The helix axis parameters for the original crystal structure and the structures attained following 100 ns molecular dynamics simulation are tabulated in Supplementary Table S3, and Table 3, respectively. All helicoidal parameters were calculated using the X3DNA software. Among these, the subset including Stretch, Shear, and Stagger are the distance parameters, represented in angstroms (Å). Upon examining the values shown in Supplementary Tables S4 & S5, it is obvious that these parameters are relatively steady, with typical values in the proximity of zero. In both the A- and B- forms of DNA, all these displacements are either zero or nearly so. Any departure from zero affects base pair stacking and may lead to instability in the complex. The erstwhile subset, including Propeller, Buckle, and Opening, the angular parameters are expressed in degrees (º). The Buckle values in Tables S4 & S5 display oscillations that are close to the pivot points. The DNA quadruplex exhibits negative propeller values for all base pairs, and the opening angles show alternating negative and positive values as is typical. A negative opening value indicates an opening toward the minor groove side. The specificity for the opening of base pairs is not discernible. The distance parameters Shift, Slide, and Rise, are measured in (Å) units. From Supplementary Tables S6 and S7, we can see that these values are close to those seen in B-form DNA, exhibiting fluctuating patterns.

Parameters– Roll, Tilt, and Twist, are reported too in Tables S6 & S7 and because the finite backbone chain length naturally causes dislocations from one base pair to the next, variations in these parameters are seen for A and B forms DNA at different phases. There are other B-DNA helices where similar relationships have been found. On the minor groove side, compression is indicated by the Roll parameter's positive sense. Roll and Tilt parameters describe the local extension of inter-base pair displacements relative to the minor groove side. The computed parameters provide insight into the dynamic behavior of the DNA quadruplex model's dynamic behavior as well as its initial structure. The data reveals that the parameters remain unchanged, indicating the stability of the quadruplex. This stability appears to persist despite the increase in atomic kinetic energy with rising temperature, which enhances vibrations and ultimately leads to the disruption of DNA quadruplexes.

TABLE 3. Local base pair helical parameters for the final structure (100.0 ns) of DNA G-quadruplex

S.N.	step	*X-disp*	*Y-disp*	*h-Rise*	*Incl.*	*Tip*	*h-Twist*
1	GT/TG	--	--	--	--	--	--
2	TG/GT	--	--	--	--	--	--
3	GG/GG	-0.6	1.65	-0.61	-73.95	-45.35	174.74
4	GG/GG	0.05	-2.44	-1.3	-58.87	-65.52	176.12
5	GG/GG	1.09	-1.31	0.02	76.42	46.09	171.25
6	GT/GG	-2.72	0.76	2.05	6.41	19.83	-33.58
7	TG/GG	--	--	--	--	….	--
8	GG/GG	1.07	-0.8	3.47	84.92	6.87	116.5

S.N.	step	*X-disp*	*Y-disp*	*h-Rise*	*Incl.*	*Tip*	*h-Twist*
9	GG/GG	-0.62	0.69	-2.69	--	8.25	157.08
10	GG/TG	--	--	…	--	--	--
11	GG/TT	--	--	--	-1.29	--	--
12	GG/TT	-0.98	-0.31	-1.81	-40.29	86.56	178.85
13	GG/GT	0.31	2.13	-4.09	-0.04	15.89	-128.51
	ave.	-0.3	0.05	-0.62	58.18	9.08	101.56

3.4. RMSD and RMSF Analysis

RMSD of the DNA helix axis is a valuable tool for analysing the dynamic and structural stability of DNA. It is a common way to compare the 3D structures of biomolecules. Its analysis provides insights into the stability and fluctuations of the helix axis. RMSD can reveal how much the helix axis fluctuates or gets distorted which can impact DNA function. Root mean square deviations (RMSD) were calculated for the MD-simulated structures at 300 K, using the initial structure as a reference for 100 ns time interval (Fig. 2). Analysis of RMSD for the quadruplex at 300 K demonstrates substantial deviations in all the planes of the model. Overall, considering the minor changes in torsion angles, and helix axis parameters, there is a noticeable convergence of the DNA quadruplex structure at 300 K, as indicated by the RMSD value of 5 Å.

The convergence and stability profiles in Fig. 2 suggest that during the simulation, the MD structure rapidly transitions to a stable equilibrium position, exhibiting relatively small oscillations centered around 5 ± 2 Å for the collective chains. Although, chain C, shows large fluctuations up to 16 Å during the initial 10 ns of MD. The RMSD plot in Fig. 2 shows that during the MD simulation at 300 K, the RMSD of the heavy atoms remains within a narrow range centered around 5 ± 2 Å for all four chains (A, B, C, and D) when the system is constrained. Chain A shows fluctuation at 25-30 ns up to 12 Å. All four strands stabilize, with the oscillation range extending from 4 to 7 Å. This suggests increased thermal fluctuations, leading to base pair perturbations. Finally, in the RMSD plot, we noted that all four chains of the quadruplex initially shifted to 5 ± 2 Å till the end of the simulation. This shift happens because removing constraints and increase of entropy enable the system to adopt a more stable conformation.

The Root Mean Square Fluctuation (RMSF) quantifies the average deviation of individual residues over time from a reference position. The RMSF profile of the DNA quadruplex structure during a molecular dynamics simulation is shown in Fig. 2. The analysis at 300 K revealed that the RMSF values for the four chains were 4 Å for chain A, 10 Å for chain B, 14 Å for chain C, and 16 Å for chain D, with significant fluctuations observed throughout the 100 ns molecular dynamics simulation indicating more flexibility of the DNA molecule making it capable of accommodating dugs and other ligands. Furthermore, the RMSF analysis indicated that chains C and D exhibited higher fluctuation values, while chains A and B remained relatively stable.

3.5. Principal Component Analysis

Essential dynamics, in terms of principal component analysis on the position of Phosphorus (P) atoms in the DNA model, was also conducted on the generated 100 ns MD simulation trajectory to understand the essential displacement of the model at simulated temperature. In Fig. 3a-d, the scree plot shows the total variance in essential displacement adopted by the extracted principal component. Herein, the first six eigenvectors, or principal components, account for most of the variance (91.2%) followed by a state of equilibrium. As first three PCs covered maximum of the substantial variance (69.8%), thus, first three PCs were considered for the further score plot analysis (Fig. 3). Analysis of extracted three PCs showed compact clusters with respect to time, which indicates no substantial displacement in the P atoms during the 100 ns MD simulation. Furthermore, the computed statistical mechanics parameters corroborated these findings such as RMSD and RMSF of the DNA model. Statistical validation using the broken stick model confirmed that the variance associated with these components exceeds that expected by chance. Additionally, bootstrap resampling (n = 1000) provided 95% confidence intervals for the variance of each PC, visualized as error bars in the cumulative variance plot (Fig. 3). The G4-quadruplex displays well-separated conformational clusters, indicating that it samples multiple stable or metastable conformations during the simulation..

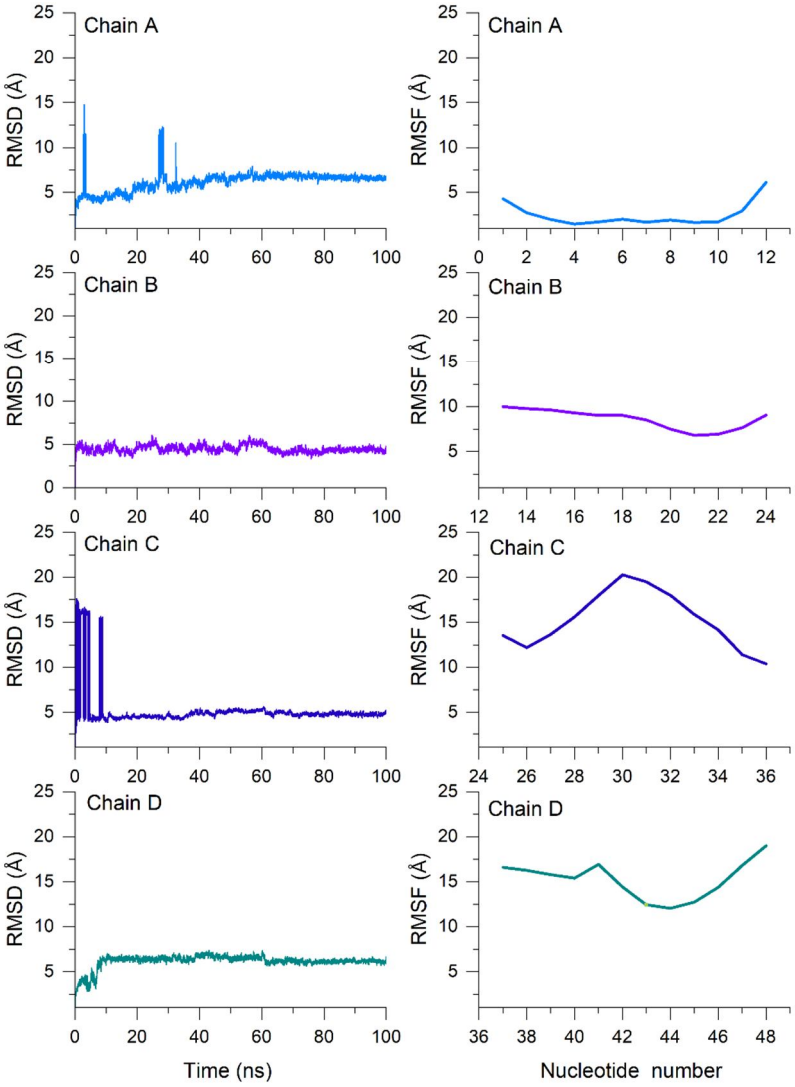

FIG. 2. RMSD and RMSF plots for the different chains of the G4 structure extracted from 100 ns MD simulation interval.

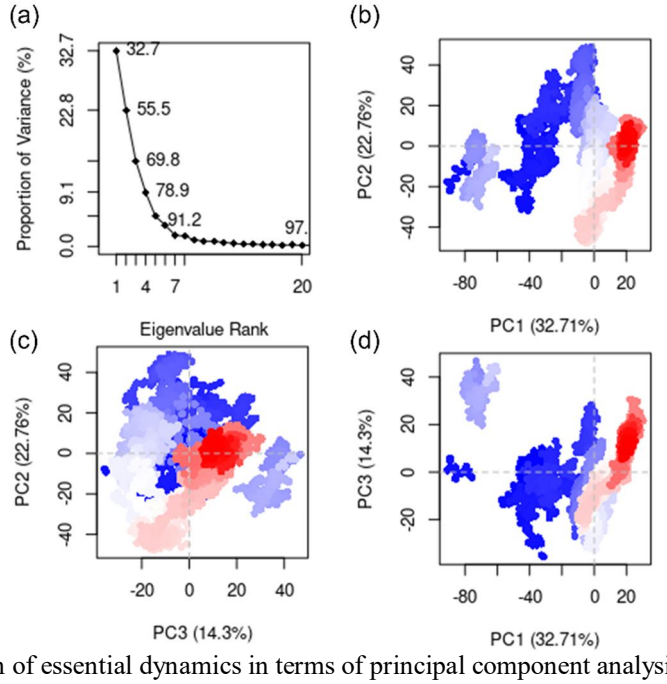

FIG. 3. Computation of essential dynamics in terms of principal component analysis on the 100 ns MD simulation trajectory of DNA model.

In the sub-Fig. 3(a), the Eigenvalue Rank on X-axis depicts the PCs and percentage of total variance computed for each PC has shown on Y-axis. The scatter plots (c-d) show the scattering of essential displacement of P- atoms among two different PCs, with color variations from red to blue through white representing the intervallic deviations knowledgeable by the P- atoms as the function of time during 100 ns simulation.

4. Conclusions

In this paper, we have taken co-ordinates of DNA quadruplex and performed a molecular dynamics simulation for 100 ns by maintaining the temperature at 300 K. The final structure obtained was compared with the initial structure as well as with the standard DNA structures. The result obtained was analyzed by taking the snapshots at periodic intervals of 10 ns for the entire trajectories of 100 ns simulation. Several observations were derived from the snapshots whereas the structural variation in conformation of the DNA molecule was obtained by calculating the torsion angle parameters and helix axis parameters which we have discussed in results. The RMSD and RMSF calculations are also mentioned to check the flexibility of the molecule and the conformational change the molecule undergoes during the course of simulation. The final observations were also compared by taking the PCA analysis. The results suggest that MD simulation of the $d(G_4T_4G_4)$ G-quadruplex at 300 K shows the B-DNA conformations which is in agreement with the experimental results of crystal structure. It maintained its structural integrity without significant unfolding, indicating the molecule's inherent flexibility. Structural fluctuations observed in the RMSD and RMSF analyses likely result from localized flexibility in the loop and terminal regions of the G-quadruplex. These regions undergo minor conformational rearrangements, such as loop bending, base flipping, and slight shifts in backbone torsion angles, which contribute to variations in helical parameters under physiological conditions. The simulation indicated that the molecule has expansion and compression characteristics, suggesting potential for receptor functionality in drug binding. The current trajectories exhibit oscillatory motions about α, β and γ torsion angles. Here we have observed that, relative to the sugar moiety, the bases can adopt orientations about the glycosidic link which is defined by the glycosidic torsion angle χ. It is seen that the χ parameter remains in the -ac region, throughout the trajectories, for all the nucleotides. In summary, DNA G-quadruplexes exhibit slight structural variations under physiological conditions in dilute aqueous solution at 300 K, maintaining overall stability. Their flexible loop regions present accessible binding sites, making them attractive targets for therapeutic intervention. These structural features are crucial for the design of G4-targeting drugs aimed at regulating gene expression and maintaining genome stability.

Acknowledgement

Jwala ji Prajapati is thankful to joint CSIR-UGC for providing the JRF/NET research fellowship. U. Yadava is thankful to the Council of Science and Technology, Uttar Pradesh, Lucknow, for financial support through its major Research Project.

Supplementary Materials

Torsion angle parameters of the initial structure:

The supplementary Tables S1 and S2 present the backbone torsion angles (**α, β, γ, δ, ε, ζ**) and glycosidic torsion angle (**χ**) for each nucleotide in the telomeric G-quadruplex DNA sequence, of the initial (i.e. crystallographic) structure corresponding to $d(G_4T_4G_4)_4$ from *Oxytricha trifallax*. Each row in the table corresponds to a nucleotide residue in the sequence, with guanine (G) and thymine (T) bases alternating in a pattern consistent with the G-quadruplex-forming motif. The backbone torsion angles describe the rotation around bonds connecting the sugar-phosphate backbone, which are critical in defining the DNA's local and global conformations. The glycosidic torsion angle (χ) indicates the orientation of the base relative to the sugar. These conformations are especially relevant for guanine residues in G-quadruplexes, where a mix of *syn* and *anti*-orientations enables the formation of the Hoogsteen hydrogen-bonded G-tetrads. Notably, several guanine residues exhibit χ torsion angles in the syn range, underscoring their involvement in tetrad formation with specific stacking geometries. In contrast, the remaining guanines predominantly adopt the anti-conformation. This alternating syn/anti pattern is characteristic of certain parallel or hybrid G-quadruplex topologies. Some torsion angle values are missing (denoted as "--"), likely due to dynamic fluctuations associated with flexible loop regions. Overall, the data highlights the structural heterogeneity and conformational diversity intrinsic to G-quadruplex DNA, supporting the sequence's capability to form stable, four-stranded helical architectures with sequence-dependent twist and stacking features.

TABLE S1. Torsion angle parameters of strand-I for the initial structure of DNA G-quadruplex

S. N.	base	*alpha*	*beta*	*gamma*	*delta*	*epsilon*	*zeta*	*chi*
1	T	144.3	163	168.8	83.9	-163.3	-30.1	-168.9
2	G	87.3	136.7	-146.7	90.9	--	--	-164.5
3	G	--	--	-93.1	134.1	178.1	-95.4	44.5
4	G	112.2	-132.8	-164.4	84	-136.9	-48	-7.5
5	G	-174.1	145.9	165.7	150.6	-129	-15.7	-165.2
6	G	-119	61.4	-171.2	100.7	153.6	38.7	-8
7	G	-115	-134.6	90.7	76.4	82.5	81.9	168.6
8	G	-174.7	85.8	143.9	89.9	158.9	-18.9	-173.4
9	T	153.9	155.1	177.5	154.2	-149.9	-71.8	-106.5
10	G	--	--	-115.1	131.7	81.2	-62.5	134.4
11	T	138.3	146.9	-153.2	75.5	-174.5	-48.7	-159.9
12	G	102.2	150	-97.6	155.4	--	--	-113.4
13	G	169.9	164.4	173.3	76.5	-159.3	-43	-13.8
14	G	-69.6	-71.2	-152.6	111	-143.4	-82	29.4
15	G	163.6	172.8	87	94.1	124.6	-79.6	-31.2
16	G	-58.4	-56.1	-158.1	84.9	-179.3	1.4	2.2
17	G	-41	160.1	62.3	119	41.6	84.7	64.6
18	G	145.7	147.6	177.1	91.8	--	--	175.6
19	T	78.6	139.8	-169	140.1	152.4	-110.4	131.7
20	G	--	--	-129.9	108.4	176.6	-121.2	17.6

TABLE S2. Torsion angle parameters of strand-II for the initial structure of DNA G-quadruplex

S.N.	base	*alpha*	*beta*	*gamma*	*delta*	*epsilon*	*zeta*	*chi*
1	T	161	-120	122.7	70.4	176.5	-84.7	-115.6
2	G	-79.7	90.3	162.3	79.5	-152.4	-30.3	-27.2
3	G	98.4	146.6	145.1	155.9	-178.4	-115	-122.7
4	G	-86.7	176.3	41.3	146	-64.8	-133	-117.5
5	G	-164.9	120.3	146.1	81.5	145.6	49.7	-37.2
6	G	97.4	136.2	-172.9	146.3	-165.2	-132	-132.1
7	G	-53.2	-60.1	-157.8	82.4	-159.6	6.2	6.1
8	G	58.7	178.2	173.2	124.7	44	62.3	91.3
9	T	127.2	128.7	-158.1	99.8	25.2	83.3	74.5
10	G	177.8	111.1	177.5	148.2	--	--	-172.6
11	T	33	-158.8	-70.1	85	-126.1	173.8	55.7
12	G	90.9	-127.2	-170.9	126	-167.1	-112.3	40
13	G	18.3	138.7	-19	161.4	-82	-126.4	-97.6
14	G	169.2	-124	158.4	88.2	-116.3	-35.2	-169.9
15	G	109.8	76	173.8	72.9	173.2	65.5	-27.2
16	G	140	114.4	167.5	141.5	147.1	92.9	-173.3
17	G	-172.2	91.6	123.9	86.3	79	58.3	-173.8
18	G	--	--	-144.4	121.3	72.6	67.4	84.6
19	T	59.3	-172.7	-143.9	149.2	-141.3	-60.6	-98.2
20	G	-134	122.9	101.3	84.4	175.7	-34.7	-166.2

Helical Parameters of Initial G-Quadruplex Structure

Table S3 summarizes key helical parameters calculated for each base step in the crystallographic (initial) structure of the telomeric G-quadruplex DNA, d($G_4T_4G_4$)$_4$, from *Oxytricha trifallax*. Parameters include X- and Y-displacement (Å), helical rise (h-Rise, Å), inclination (Incl., °), tip (°), and helical twist (h-Twist, °), which together describe the spatial arrangement and local geometry of successive base pairs or tetrads.

The majority of steps involve guanine–guanine (GG/GG) pairs, which form the G-tetrads essential to the G-quadruplex core. These steps exhibit substantial variability in inclination

and tip angles, reflecting the non-canonical, non-uniform stacking typical of G-quadruplex DNA. Notably, steps 3, 5, 7, 12, 14, and 16 show particularly large deviations in inclination and tip, indicating localized structural distortions or twisting within the quadruplex stack. Missing values ("--") at steps 8, 10, and 19 correspond to thymine-rich loop regions (GT/TG or TG/GT steps) where base pairing is absent in the crystal structure, likely due to high flexibility or disorder. The average values (bottom row) highlight an overall modest displacement and rise per step, but large standard deviations (especially in inclination and tip) emphasize the significant conformational diversity across the quadruplex. The mean h-Twist (~102.64°) reflects an overall right-handed helical winding, though the high standard deviation (131.06°) again underscores irregularity in stacking geometry. Together, these metrics illustrate the non-uniform yet stable nature of the G-quadruplex scaffold, with alternating structured tetrads and flexible loops.

TABLE S3. Local base pair helical parameters for the initial structure (0.0 ns) of DNA G-quadruplex

S. N.	step	*X-disp*	*Y-disp*	*h-Rise*	*Incl.*	*Tip*	*h-Twist*
1	TG/GT	-1.34	-0.51	-3.75	-0.42	1.21	140.68
2	GG/GG	-2.02	0.09	-0.62	-6.38	6.26	176.88
3	GG/GG	0.27	2.01	-2.28	-35.22	81.46	171.88
4	GG/GG	-1.76	0.72	0.89	6.4	-6.09	175.33
5	GG/GG	-1.56	-0.03	-0.65	-14.27	87.13	178.97
6	GG/GG	-1.89	0.3	-0.63	2.08	4.19	175.51
7	GG/GG	-2.01	0.75	0.8	39.04	-77.91	170.25
8	GT/TG	--	--	--	--	--	--
9	TG/GT	-0.71	0.57	-3.62	0.66	-0.37	128.71
10	GT/TG	--	--	--	--	--	--
11	TG/GT	-0.06	-2.26	-3.84	-4.99	-2.83	114.86
12	GG/GG	-1.28	1.02	-2.03	-79.36	-33.37	-175.56
13	GG/GG	-1.71	1.02	1.29	7.67	-1.34	167.73
14	GG/GG	1.41	1.03	1.29	17.43	-86.86	-177.09
15	GG/GG	-1.87	0.4	-0.55	2.31	7.05	173.91
16	GG/GG	-1.79	0.25	1.42	34.38	-78.51	168.53
17	GG/GG	-2.05	0.19	0.24	-2.79	-0.33	172.39
18	GT/TG	-0.4	1.27	3.46	2.4	-3.76	-120.81
19	TG/GT	--	--	--	--	--	--
	ave	-1.17	0.43	-0.54	-1.94	-6.5	102.64
	s.d.	1.01	0.93	2.11	26.93	48.04	131.06

Base Pair Parameters of the Initial Quadruplex Structure:

Table S4 summarizes base pair parameters - shear, stretch, stagger (Å), and buckle, propeller, opening (°)—for the initial crystallographic structure of the telomeric G-quadruplex $d(G_4T_4G_4)_4$. The G+G Hoogsteen pairs within the tetrads display large propeller twists and opening angles (often >± 80°), along with significant buckle values, reflecting non-canonical geometry essential for tetrad stacking. Loop-associated T–T and mixed pairs show high variability, with extreme distortions in entries like S.N. 11 and 19, indicative of local flexibility. Overall, the data highlight the structural heterogeneity of G4 DNA, with a stable tetrad core and dynamic loop regions essential for its biological function.

TABLE S4. Local base pair parameters for the initial structure (0.0 ns) of DNA G-quadruplex

S.N.	bp	*shear*	*stretch*	*stagger*	*buckle*	*propeller*	*opening*
1	T-T	-5.33	-0.98	0.09	13.17	-15.18	38.07
2	G+G	-2.39	-2.56	-0.64	-16.79	5.07	86.21
3	G+G	1.64	2.51	1.66	1.72	-12.41	-89.4
4	G+G	-0.15	3.7	-2.15	22.64	-9.97	-97.02
5	G+G	0.1	-4.28	0.22	-0.56	-12.8	90.53
6	G+G	-2.24	-3.81	0.17	-10.35	1.92	83.76

S.N.	bp	*shear*	*stretch*	*stagger*	*buckle*	*propeller*	*opening*
7	G+G	1.68	3.87	0.47	-13.26	-6.24	-87.21
8	G+G	1.51	3.66	-0.4	-0.46	-2.95	-92.84
9	T+T	7.03	1.5	-0.95	17.73	-10.71	-6.28
10	G+G	-1.69	-3.85	0.09	6.45	-18.82	76.98
11	T+T	-6.58	5.73	-0.04	14.21	5.03	-41.76
12	G+G	-2.54	-3.11	0.02	11.25	-0.31	85.19
13	G+G	0.53	3.89	-2.4	26.29	-8.98	-92.41
14	G+G	-0.91	4.83	-0.08	-5.29	2.61	-101.18
15	G+G	2.3	3.04	0.68	1.09	-7.65	-90.96
16	G+G	-1.76	-3.37	-0.75	12.04	-0.49	83.89
17	G+G	-3.22	-3.13	0.1	-6.27	-2.95	78.5
18	G+G	2.34	3.13	1.24	-29.2	5.05	-82.9
19	T+T	-6.86	1.07	0.51	-6.66	40.51	10.68
20	G+G	1.87	2.25	2.17	-10.36	-1.7	-89.9

Base Pair Parameters of the quadruplex after 100 ns MD Simulation

Table S5 summarizes the base pair parameters of the telomeric G-quadruplex d($G_4T_4G_4$)$_4$ after 100 ns of molecular dynamics simulation, capturing shear, stretch, stagger (Å), and buckle, propeller, and opening (°). G+G tetrad pairs (e.g., S.N. 1, 4, 6, 10, 14) maintain large angular distortions characteristic of Hoogsteen pairing, with notable propeller twists (±40° to –50°) and high opening values. Loop and junction pairs (e.g., T–T, T–G, G–T, G+T) show increased variability, with opening angles ranging from –85° to +175°, indicating dynamic flexibility. While average shear and stretch remain modest, the elevated mean opening angle (+20.21°) reflects persistent local breathing. These findings highlight the structural adaptability of G4 DNA, balancing tetrad stability with loop-region flexibility.

TABLE S5. Local base pair parameters for the final structure (100.0 ns) of DNA G-quadruplex

S.N.	bp	*shear*	*stretch*	*stagger*	*buckle*	*propeller*	*opening*
1	G+G	1.9	3.27	0.86	37.65	-37.33	-81.32
2	T-T	3.49	0.16	-0.86	6.06	12.39	66.14
3	G+G	-1.77	-3.98	-0.33	4.16	20.09	78.72
4	G+G	2.08	3.26	0.42	-30.16	2.63	-85.19
5	G+G	-2.16	-3.2	-0.38	29.16	-4.02	82.88
6	G+G	1.77	3.36	0.2	-9.54	-40.96	-79.2
7	T-G	-4.1	1.14	-1.22	39.74	-42.69	11.69
8	G+G	2.6	2.77	-0.23	21.96	34.45	-78.02
9	G+G	-2.41	-2.64	0.31	-12.56	-24	87.94
10	G+G	6.28	-5.01	0.32	-14.84	-52.74	177.29
11	G-T	2.73	1.97	-1.51	31.78	-0.55	49.09
12	G+T	6.74	-4.1	-1.22	-33.1	-32.32	81.4
13	G-T	-1.74	-0.14	0.76	-27.58	47.33	-24.89
14	G+G	-6.61	-3.71	-0.37	-5.81	-7.89	-3.56
	ave.	0.63	-0.49	-0.23	2.64	-8.97	20.21

Local Base Pair Step Parameters of the Initial Structure:

Table S6 summarizes base pair step parameters: Shift, Slide, Rise (Å) and Tilt, Roll, Twist (°) for the initial crystal structure of the telomeric G-quadruplex, d($G_4T_4G_4$)$_4$. These values capture the stacking interactions and helical deformations between adjacent base pairs. GG/GG steps, forming the G-tetrads, display large deviations in angular parameters (e.g., extreme Tilt and Roll), consistent with the non-canonical Hoogsteen pairing and distorted stacking geometry of G4 DNA. Twist angles vary widely, indicating irregular helical winding. TG/GT and GT/TG steps, found in loop regions, show irregular or missing values, reflecting local flexibility or disorder. The data highlights a structurally heterogeneous scaffold: rigid, stacked tetrads interspersed with dynamic, flexible loops—key to G-quadruplex folding and function.

TABLE S6. Local base pair step parameters for the initial structure (0.0 ns) of DNA G-quadruplex

S.N.	Step	*Shift*	*Slide*	*Rise*	*Tilt*	*Roll*	*Twist*
1	TG/GT	0.99	-2.52	-3.75	-2.28	-0.79	140.68
2	GG/GG	-0.18	-4.03	-0.64	-12.52	-12.76	176.84
3	GG/GG	0.24	2.37	-3.98	-157.42	-68.06	34.12
4	GG/GG	-1.43	-3.51	0.91	12.17	12.79	175.28
5	GG/GG	0.26	-3.08	-0.75	-174.11	-28.51	146.42
6	GG/GG	-0.6	-3.77	-0.62	-8.37	4.15	175.5
7	GG/GG	0.5	-3	3.11	150.82	75.58	60.56
8	GT/TG	--	--	--	--	--	--
9	TG/GT	-1.03	-1.29	-3.61	0.67	1.19	128.7
10	GT/TG	--	--	--	--	--	--
11	TG/GT	3.71	0.09	-3.94	4.77	-8.4	114.6
12	GG/GG	1.74	3.3	-0.99	-66.28	157.63	-120.79
13	GG/GG	-2.03	-3.39	1.34	2.67	15.25	167.62
14	GG/GG	2.54	-2.73	-0.15	-172.51	-34.63	-88.08
15	GG/GG	-0.79	-3.73	-0.54	-14.08	4.6	173.86
16	GG/GG	1.24	-2.8	2.35	151.76	66.46	73.42
17	GG/GG	-0.37	-4.09	0.23	0.66	-5.57	172.38
18	GT/TG	2.33	0.77	3.37	-6.53	-4.17	-120.66
19	TG/GT	--	--	--	--	--	--

Local Base Pair Step Parameters of the 100 Ns MD Simulated Structure:

Table S7 summarizes base pair step parameters—Shift, Slide, Rise (Å), and Tilt, Roll, Twist (°) for the telomeric G-quadruplex after 100 ns of molecular dynamics. GG/GG steps in the G-tetrad core exhibit highly distorted angular values (Tilt ±130°, Roll ±150°), indicating major stacking rearrangements while preserving tetrad integrity. Twist varies widely (19° to 160°), reflecting local helix distortion. Missing values for loop/ junction steps (e.g., GT/TG, GG/TT) suggest high flexibility or disruption. An average negative Rise (–0.48 Å) and large deviations, point to stacking irregularities and possible strand slippage. Overall, the data highlight the structural plasticity of G-quadruplexes, stable yet dynamically distorted cores with flexible loops, key to their biological function and ligand adaptability.

TABLE S7. Local base pair step parameters for the final structure(100ns) of the quadruplex

S.N.	*step*	*shift*	*slide*	*rise*	*tilt*	*roll*	*twist*
1	GT/TG	--	--	--	--	--	--
2	TG/GT	--	--	--	--	--	--
3	GG/GG	-3.42	-1.01	-0.03	89.73	-146.31	102.06
4	GG/GG	3.39	1.42	-3.45	129.84	-116.67	89.2
5	GG/GG	2.82	1.82	-0.5	-88.38	146.53	19.46
6	GT/TG	-0.23	1.79	1.9	11.23	-3.63	-31.5
7	TG/GT	--	--	--	--	--	--
8	GG/GG	1.15	2.02	3.44	-11.68	10.7	115.81
9	GG/GG	-1.17	-3.02	-0.03	-15.01	154.54	43.87
10	GG/TG	--	--	--	--	--	--
11	GG/TT	--	--	--	--	--	--
12	GG/TT	0.91	-1.96	-169	-173.03	-2.58	160.89
13	GG/GT	4.38	0.82	-3.45	28	71	-112.93
	ave	0.98	0.23	-0.48	-3.66	14.2	48.36

6. References

[1] Burge, S., Parkinson, G.P., Hazel, P., Todd, A.K., and Neidle, S., Nucleic Acids Research, 34 (2006) 5402.

[2] Spiegel, J., Adhikari, S., and Balasubramanian, S., Trends in Chemistry, 2 (2020) 123.

[3] Lipps, H.J., Gruissem, W., and Prescott, D.M., Proceedings of the National Academy of Sciences of the USA, 79 (8) (1982) 2495.

[4] Kang, C., Zhang, X., Ratliff, R., Moyzis, R., and Rich, A., Nature, 356 (1992) 126.

[5] Rawal, P., Kummarasetti, V.B., Ravindran, J., Kumar, N., Halder, K., Sharma, R., Mukerji, M., Das, S.K., and Chowdhury, S., Genome Research, 16 (5) (2006) 644.

[6] Perrone, R., Nadai, M., Poe, J.A., Frasson, I., Palumbo, M., Palù, G., Smithgall, T.E., and Richter, S.N., PLoS One, 8 (8) (2013) e73121.

[7] Garg, R., Aggarwal, J., and Thakkar, B., Scientific Reports, 6 (1) (2016) 1.

[8] Largy, E., Mergny, J.L., and Gabelica, V., Metal Ions in Life Sciences, 16 (2016) 203.

[9] Yadav, V., Kim, N.H., Tuteja, N., and Yadav, P., Frontiers in Plant Science, 8 (2017) 1163.

[10] Robert, C., Monsen, J.O.T., and Jonathan, B.C., Accounts of Chemical Research, 55 (22) (2022) 3242.

[11] Perrone, R. et al., Scientific Reports, 7 (2017) 5743.

[12] Deiana, M. et al., Nucleic Acids Research, 51 (12) (2023) 6264.

[13] Shu, H., Zhang, R., Xiao, K., Yang, J., and Sun, X., Biomolecules, 12 (5) (2022) 648.

[14] Rhodes, D. and Lipps, H.J., Nucleic Acids Research, 43 (2015) 8627.

[15] Rawal, P. et al., Genome Research, 16 (5) (2006) 644.

[16] Wu, G. et al., Molecules, 25 (15) (2020) 3465.

[17] Ruggiero, E. and Richter, S.N., Bioorganic & Medicinal Chemistry Letters, 79 (2023) 129085.

[18] Sun, D. and Hurley, L.H., Journal of Medicinal Chemistry, 52 (2009) 2863.

[19] Villar-Guerra, R.D. et al., Angewandte Chemie International Edition, 130 (24) (2018) 7289.

[20] Castelli, M. et al., Journal of Chemical Theory and Computation, 18 (7) (2022) 4515.

[21] Lombardi, E.P. and Vallejo, L., Nucleic Acids Research, 48 (3) (2019) 1603.

[22] Moraca, F. et al., Proceedings of the National Academy of Sciences of the USA, 114 (11) (2017) E2136.

[23] Salgado, G.F. et al., Chemical Science, 6 (2015) 3314.

[24] Tiago, S. et al., Pharmaceuticals, 14 (8) (2021) 769.

[25] Yadav, R.K. and Yadava, U., Medicinal Chemistry Research, 23 (1) (2014) 280.

[26] Yadava, U. et al., DNA Repair, 60 (2017) 9.

[27] Yadava, U. et al., Journal of Molecular Liquids, 280 (2019) 135.

[28] Yadav, R.K. and Yadava, U., Bioinformation, 10 (2014) 394.

[29] Yan, B. et al., International Journal of Molecular Sciences, 26 (4) (2025) 1591.

[30] Abascal, J.L.F. and Vega, C., Journal of Chemical Physics, 123 (2005) 234505.

[31] Bowers, K.J. et al., Proceedings of the ACM/IEEE International Conference on Supercomputing, (2006).

[32] Negi, S. and Yadava, U., Journal of Molecular Liquids, 412 (2024) 125825.

[33] Negi, S. et al., Journal of Biomolecular Structure and Dynamics, 2023 (2023) 1.

[34] Lu, C. et al., Journal of Chemical Theory and Computation, 17 (7) (2021) 4291.

[35] Darden, T. et al., Structure, 7 (3) (1999) R55.

[36] Bufolo, G.N. and Sobral, Y.D., Advances in Computational Mathematics, 50 (2024) 82.

[37] Grant, B.J. et al., Protein Science, 30 (1) (2021) 20.

[38] Singh, A. et al., PLoS One, 18 (2) (2023) e0278755.

[39] Greenacre, M. et al., Nature Reviews Methods Primers, 2 (1) (2022) 1.

[40] Lawson, C.L. et al., Nucleic Acids Research, 52 (D1) (2024) D245.

[41] Sundaresan, S. et al., ACS Omega, 9 (37) (2024) 38696.

[42] Kosiol, N. et al., Molecular Cancer, 20 (2021) 40.

[43] Frasson, I. et al., International Journal of Biological Macromolecules, 204 (2022) 89.

[44] Batool, M. et al., International Journal of Molecular Sciences, 20 (2019) 2783.

[45] Šponer, J. et al., Annual Reports in Medicinal Chemistry, 54 (2020) 197.

[46] Šponer, J. et al., Methods, 57 (2012) 25.

[47] Ivani, I. et al., Nature Methods, 13 (2016) 55.

[48] Liu, Y. et al., Journal of the American Chemical Society, 145 (2023) 16228.

[49] Farag, M. et al., Nucleic Acids Research, 51 (5) (2023) 2087.

[50] Prajapati, J.J. et al., Prabha Materials Science Letters, 4 (1) (2025) 107.